Insertion and Confinement of H 2 O in Hydrophobic Siliceous Zeolites at High Pressure

Mario Santoro, Vasyl Veremeienko, Michelangelo Polisi, Riccardo Fantini, Frederico Alabarse, Rossella Arletti, Simona Quatieri, Volodymyr Svitlyk, Arie van Der Lee, Jérôme Rouquette, et al.

Insertion and Confinement of H_2O in Hydrophobic Siliceous Zeolites at High Pressure

Mario Santoro[°■], *Vasyl Veremeienko*[†], *Michelangelo Polisi*[§], *Riccardo Fantini*[§], *Frederico Alabarse*[‖], *Rossella Arletti*[‡], *Simona Quatieri*[⊥], *Volodymyr Svitlyk*[▽], *Arie van der Lee*[□], *Jérôme Rouquette*[†], *Bruno Alonso*[†], *Francesco Di Renzo*[†], *Benoît Coasne*[▲], *Julien Haines**[†]

[°]Istituto Nazionale di Ottica, CNR-INO, 50019 Sesto Fiorentino, Italy.

[■]European Laboratory for Non Linear Spectroscopy (LENS), 50019 Sesto Fiorentino, Italy.

[†]ICGM, CNRS, Université de Montpellier, ENSCM, Montpellier, France.

[§]Dipartimento di Scienze Chimiche e Geologiche, Università di Modena, Modena, Italy

[‖]Elettra Sincrotrone Trieste, Trieste, Italy

[‡]Dipartimento di Scienze della Terra, Università di Torino, Torino, Italy

[⊥]Dipartimento di Scienze Matematiche e Informatiche, Scienze Fisiche e Scienze della Terra, Università di Messina, Messina, Italy

[▽]ESRF, 38000 Grenoble, France.

[□]IEM, CNRS, Université de Montpellier, Montpellier, France

[▲]Université Grenoble Alpes, CNRS, LIPhy, Grenoble, France

ABSTRACT

The insertion of H_2O in the siliceous zeolites TON (Theta-one) and MFI (Mobil-Five) was studied at pressures up to 0.9 GPa by synchrotron X-ray diffraction, infrared spectroscopy and Monte Carlo Modeling. TON (orthorhombic, $Cmc2_1$) and MFI (monoclinic, $P2_1/n$) have 1D and 3D pore systems respectively. H_2O insertion was quantified by a combination of structure refinements and Monte Carlo modelling. Complete pore filling is observed at 0.9 GPa in the high-pressure forms of TON (orthorhombic, $Pbn2_1$) and MFI (orthorhombic, *Pnma*). This corresponds to more than twice as many H_2O molecules per SiO_2 unit in the 3D pore system of MFI than in the 1D pore system of TON. This results in a greater swelling of the MFI system as compared to the TON system upon insertion. In both cases, both experiments and modelling indicate that the density of water in the pores is close to that of bulk water at the same pressure. A greater degree of molecular disorder is observed in the 3D network of MFI. Infrared spectroscopy indicates a weakening of the hydrogen bonds associated with geometrical constraints due to confinement. The majority of the H_2O molecules are extruded on pressure release indicating that this insertion is reversible to a great extent, which gives rise to the molecular spring properties of these materials.

1. Introduction

The penetration of H_2O in porous materials is of great importance for chemistry, materials and Earth science. Water penetration strongly modifies the properties of materials and minerals and has implications for energy storage, aging of materials, and geological processes. Particular interest has been directed towards microporous zeolite-type materials with typical diameters between 3-8Å, for which it has been shown that high pressure can lead to a superhydrated state[1-10]. This effect strongly modifies the phase stability and the elastic properties of these materials. Hydrophobic, all silica zeolites coupled to non-wetting fluids are particularly suited for applications for the storage, absorption, and dissipation of mechanical energy for use as molecular springs, bumpers and shock absorbers[11-18].

One of the most studied siliceous zeolites for such applications, both from an experimental and computational point of view, is silicalite-1 with a MFI structure[19]. This material is characterized by a three dimensional pore system consisting of 5.1×5.5Å diameter straight channels along the [010] direction and intersecting 5.3×5.6Å sinusoidal channels in the *ac* plane. This phase is known to undergo a monoclinic to orthorhombic phase transition as a function of temperature, pressure and guest insertion[20-22]. Porosimetric studies revealed that, once H_2O is intruded in silicalite-1 a reversible-penetration of molecules occurs close to 100 MPa[11, 18] with some hysteresis.

Superior energy storage properties have been observed for an orthorhombic 1-D siliceous zeolite TON, which has unidirectional 4.6×5.7Å elliptical channels along the [001] direction[23-25]. Penetration by water molecules occurs at 186 MPa[17]. This material undergoes a pressure-induced phase transition between $Cmc2_1$ and $Pbn2_1$ orthorhombic forms[26] at close to 700 MPa. This transition occurs in non-penetrating hydrostatic pressure transmitting media, but it is also observed with a lower degree of distortion in the presence of guest atoms such as Ne or Ar[27]. This phase transition is a consequence of the collapse of the pores along opposite diagonals[26].

The goal of the present study is to investigate the mechanism of pore filling of TON and MFI by H_2O at high pressure from a structural point of view using a combination of in situ X-ray powder diffraction and Monte Carlo modelling and also from a vibrational point of view by infrared spectroscopy.

2. Experimental and theoretical methods

Micron-sized crystals of TON were prepared by sol-gel techniques using triethylenetetramine as the structure directing agent followed by crystallization at 170°C under hydrothermal conditions and then calcination at 600°C[26, 28-29]. The Si:Al ratio of the crystals was found to be 50. Chemical analysis showed that the material contained 0.41%N and 0.37%C corresponding to a residue from the calcined structure directing agent and 0.3% Na from the starting gel. The nitrogen adsorption isotherm indicated that 100% of the porosity was available. The initial unit cell parameters obtained on a Panalytical X'Pert diffractometer using Cu Kα radiation were: a=13.8652(1)Å, b=17.4233(3)Å, c=5.03928(7)Å in space group $Cmc2_1$. MFI crystals were also prepared by sol-gel techniques in the presence of ammonium fluoride using fumed silica as the silica source and tetrapropylammonium bromide as the structure directing agent. Crystallization was obtained under hydrothermal conditions at 200°C for 15 days and was followed by calcination at 550°C. The resulting crystals were finely ground down to micron size under wet conditions using a McCrone™ X-ray diffraction mill. The initial unit cell parameters obtained on a Bruker D8 Discover diffractometer using Cu Kα1 radiation were: a=20.1344(1)Å, b=19.9018(1)Å, c=13.38641(8)Å, α=90.6207(5) in the non-standard setting of the space group $P2_1/n$ ($P2_1/n11$) in order to retain the same axes as the orthorhombic aristotype *Pnma*.

X-ray powder diffraction (λ=0.3738 Å) experiments were performed in a LENS membrane-type diamond anvil cell (DAC) on the ID27 High Pressure beamline at the ESRF synchrotron (Grenoble, France) using a MAR165 CCD detector. We first homogeneously filled the 300 µm diameter hole of a 70 µm thick indent in a stainless steel gasket with hydrophobic micron-sized TON or MFI powder, and the powder was just gently compacted in order not to prevent the subsequent loading of water. A ruby microsphere

was added as pressure calibrant. A drop of ultrapure water was then added as pressure transmitting medium, which filled both the pores of the zeolite (confined H_2O) and the residual empty space between the grains of the zeolite (bulk H_2O). Pressure was measured based on the shift of the ruby R_1 fluorescence line[30]. The diffraction patterns were analyzed and integrated using the Dioptas 0.4.0 program[31]. Rietveld refinements were performed using the program Fullprof[32]. Fractional atomic coordinates for the framework from previous work were used as the starting model for TON[26]. In the case of MFI, the starting fractional atomic coordinates were obtained from an x-ray diffraction study of a single-crystal synthesized under similar conditions. Soft constraints were applied to the Si-O distances, O-O distances and/or the O-Si-O angles. As it was not possible to locate the hydrogen atoms of the H_2O molecules and in order to correctly account for the number of electrons associated with these H_2O molecules, the scattering curve of isoelectronic neon was used in the refinements. An overall isotropic atomic displacement parameter (ADP) was used for all framework Si and O atoms and extraframework H_2O molecules as no improvement was obtained using individual ADPs. Crystal structures were plotted using the program VESTA[33]. IR absorption spectra on the H_2O/zeolite mixtures were measured by a Bruker IFS-120 HR Fourier transform infrared spectrometer equipped with a globar lamp, a KBr beam splitter, an MCT detector, and an optical beam condenser based on ellipsoidal mirrors providing a natural beam spot size of several hundreds of microns (see Gorelli et al.[34] and references therein). The typical spectral resolution was 1 cm^{-1}.

Monte Carlo simulations in the Grand Canonical ensemble (GCMC) were performed to determine the number and structure of water confined at room temperature in TON and in MFI zeolites. These atom-scale simulations at constant chemical potential μ, volume V, and temperature T allow determining the number of adsorbed water molecules, $n_{H2O}(\mu)$, per zeolite unit cell as a function of chemical potential μ[35]. For a given μ and T, the corresponding pressure P was obtained according to the data by Desbiens et al.[12] The pressures (or chemical potential) and unit cell parameters obtained from the experiments were used to perform these molecular simulations. A TON structure made of 2 × 2 × 5 rigid unit cells and a MFI

structure made of 2 × 2 × 3 rigid unit cells were considered and periodic boundary conditions were used along the x, y, z directions to avoid finite size effects. Water was described in these atom-scale simulations using the TIP4P potential, which can be assumed to be appropriate in the pressure range up to 1 GPa. Following previous work[12], interactions between water and the zeolite consisted of a Lennard-Jones potential and a Coulomb contribution (partial charges on the O and Si atoms of the pure silica zeolites are taken equal to -1e and +2e, respectively). For the Lennard-Jones potential, the cross parameters σ and ε were determined by combining the like-atom parameters using the Lorentz – Berthelot rules (the like-atom parameters for the O atom in zeolite are $\sigma = 0.3$ nm and $\varepsilon/k_B = 93.53$ K).

3. Results and discussion

The two zeolite powders TON and MFI were compressed in H_2O up to 0.9 GPa, just below the solidification pressure of ice VI[36]. X-ray diffraction measurements were then performed on pressure release (Figure 1). In both cases the diffraction patterns clearly showed that both materials underwent phase transitions to their high pressure polymorphs with space groups $Pbn2_1$ for TON and *Pnma* for MFI. At high pressure, the relative intensities of the diffraction lines were strongly modified with respect to those observed at ambient pressure, clearly indicating the insertion of H_2O. The high pressure forms were retained during the measurements on decompression, with the exception of that at ambient pressure, for which both reverted to their low-pressure forms ($Cmc2_1$ for TON and $P2_1/n11$ for MFI) with major changes in relative intensities indicative of significant extrusion of H_2O.

The structure of TON was thus refined (Figures 2 and 3, and CIF files in SI) using the above structural models for the high pressure and ambient pressure measurements respectively. Starting from the high-pressure point at 0.90 GPa, the $Pbn2_1$ structure of empty TON was used in the initial stages of the Rietveld refinement. At the highest pressure investigated, difference Fourier maps allowed two sets of 4*a* Wyckoff sites (*x,y,z*) with an occupation of 0.89(4) to be located, giving close to 8 H_2O molecules per unit cell and thus 4 in each pore. The difference between the refined occupancy and full occupation is probably due to

the C, N and Na remaining in the pores after calcination and detected by chemical analysis and any disorder present in the H_2O distribution in the channels. The corresponding electron density was accounted for in the refinement as in previous studies[26-27] by in this case on average 0.5 carbon atoms per unit cell. The configuration of sites occupied by the H_2O molecules is consistent with two hydrogen bonded chains per pore (Figure 4 and CIF files in SI). The structure is in good agreement with the results of the MC simulations, which give a maximum of 8.9 molecules per unit cell at the maximum pressure. The amount of H_2O molecules hosted in the channels decreases upon decompression at a similar rate in the experimental data and in the MC simulations (Figure 5). At ambient pressure, refinements indicated the presence of residual H_2O. The refinement allows 2.5 H_2O molecules per unit cell to be located on a set of 4*a* Wyckoff sites (0,*y*,*z*). The amount of residual water can be related to the presence of sodium cations (0.3%) and protons needed to compensate the charge of the framework containing 2% Al and to the eventual formation of silanol groups at high pressure.

Due to the complexity of the MFI structure with a much larger unit cell and a 3D pore system, the data were not of sufficient quality to determine the positions of the H_2O molecules in the pores by difference Fourier maps. H_2O molecules with soft constraints set to an approximate hydrogen-bond O-O distance of 2.8 Å were placed in a periodic way in the pores based on the results of MC models (see below) to build an initial structural model. Very good fits in Rietveld refinements were obtained with this structural model (Figure 2 and CIF files in SI). This periodic structural model used for the Rietveld refinements can readily be used to account for the electron density in the pores in terms of occupation by water molecules with a maximum of 16.6 molecules/24 SiO_2 at 0.86 GPa. On pressure release, some residual molecules H_2O (1.4 molecules/24 SiO_2) are found in the MFI channels. This amount of residual H_2O irreversibly absorbed in this hydrophobic MFI is significantly lower than the H_2O uptake in hydrophilic MFI (3 molecules/24 SiO_2), but higher than the uptake of hydrophobic MFI (0.4 molecules/24 SiO_2) in adsorption isotherm measurements[37]. This residual H_2O content could be linked to the formation of silanol groups at very high

pressures as found in previous work[14-15] in spite of the hydrophobic nature of calcined MFI obtained by the fluoride route, which is preserved from the creation of silanol defects during the calcination process. The present result indicates that the concentration of silanol defects is dramatically increased by compression up to 0.9 GPa.

The experimental H_2O content measured in this study are in excellent agreement with the points at low pressure obtained in previous volumetric studies (Figure 5); however, a much larger number of H_2O molecules enter the pores up to the maximum pressure reached in the present study. If instead of quantifying the number of guests with respect to the number of framework atoms, the data are plotted as a function of the degree of pore filling at 0.9 GPa (Figure 5b), assuming that a maximum attainable H_2O density in the pores of 1.23 g/cm^3 corresponding to that of liquid H_2O at the same pressure[38], the points of both materials lie on the same curve. The water density value attained at 0.9 GPa in the case of TON is 1.09(4) g/cm^3, whereas the maximum value for MFI is 1.17(6) g/cm^3 at 0.86 GPa. The lower value for TON can be related to the presence of the remaining C, N and Na atoms, which take the place of H_2O molecules. The results of MC simulations (see below) confirm that the density of inserted H_2O in both materials is essentially equivalent to that of liquid water at the same pressure. These results indicate that at high enough pressure, full pore filling occurs in hydrophobic zeolites. This process is reversible to a very large extent and the majority of the water is extruded on pressure release. The residual H_2O content is higher for TON (32%) as compared to MFI (8%), which can be linked to Na cations and protons in the pores, which compensate the charges due to the Al cations in the framework.

In both materials the unit cell parameters (except *b* in TON, see below) are larger than those of the corresponding empty zeolites[27, 39] compressed in non-penetrating media from 0.9 down to 0.6 GPa due to swelling of the pores induced by the presence of H_2O molecules (Figures 6 and 7). In the case of TON, the difference between the *a* and *b* parameters is greater due to greater distortion of the pores giving a

very marked decrease in *b* at the phase transition. The recovered TON has essentially identical cell parameters and volume of the empty TON. The behavior of MFI is different. Upon pressure release, the unit cell remains slightly contracted, which is consistent with the residual H_2O content and to models showing a slight collapse in zeolite structures in some cases when a layer of molecules is adsorbed on the inner surface of the pores[40].

The amount of adsorbed water in the MFI and TON structures was determined using MC simulations in the Grand Canonical ensemble. When normalized per number of SiO_2 units in the zeolites, we find 8.00, 8.59 and 8.89 H_2O per 24 SiO_2 units for TON at 0.29, 0.6 and 0.9 GPa and 13.43, 15.21 and 15.95 H_2O per 24 SiO_2 units for MFI at 0.3, 0.67 and 0.8 GPa. As can be seen in Fig. 5, these values are in very good agreement with the experimental data. In the case of MFI, these numbers are slightly larger than those predicted by Desbiens et al.[12]. Typically, at 300 MPa, we find 53.7 H_2O per unit cell in MFI instead of 49 H_2O per unit cell in Ref. 12. Such differences can be due to the model used to describe the water molecule and its interaction with the host silica zeolite – typically, the partial charges carried by the atomic sites in water and in the zeolite but also the Lennard-Jones parameters considered. For instance, in Ref. 12, upon considering different water models, the authors observed important differences in terms of the amount of water adsorbed with values at P = 350 MPa that can vary from 47 to 52 H_2O per unit cell (see Fig. 7 in Ref. 12). As for water in TON, our results are in qualitative agreement with those from Bushuev and Sastre[16] who found a maximum of 27 H_2O molecules for a TON channel, equivalent to 4 times the unit cell along the c-axis (therefore leading to about 7 water molecules per unit cell, in fair agreement with the value of 8 H_2O per unit cell found in the present work). It can be noted that in the previous study, the high-pressure phase transition in TON had not yet been discovered and was thus not considered in the calculation.

Converting the calculated number of water molecules per unit cell into a density of confined water is a complex task as the porous volume is an ill-defined quantity since its determination is probe- and/or technique-dependent. In the present work, we used the following approach. The porous volume for each zeolite was taken from the work by Krishna and Van Baten who used an in-silico screening of different zeolite materials including TON and MFI[41]. These authors evaluated the accessible pore volume by a Connolly-surface approach using He as a probe. The values given are in excellent agreement with experimental O_2 and N_2 adsorption data on silicalite[42] and TON[28]. While these values were obtained for the unstrained structures at ambient pressure conditions, we estimated the porous volume at the different pressures considered here by assuming that the porous volume V_p scales like the volume V of the sample, i.e. $V_p/V_{p,0} \sim V/V_0$. Using $V_0 \sim 231.4$ Å^3 for TON and $V_0 \sim 1584.9$ Å^3 for MFI. Considering the different strains estimated for the different pressure conditions, we obtained 1.06, 1.16 and 1.21 g/cm^3 for TON at 290, 600 and 900 MPa and 1.03, 1.18 and 1.24 g/cm^3 for MFI at 300, 670 and 800 MPa.

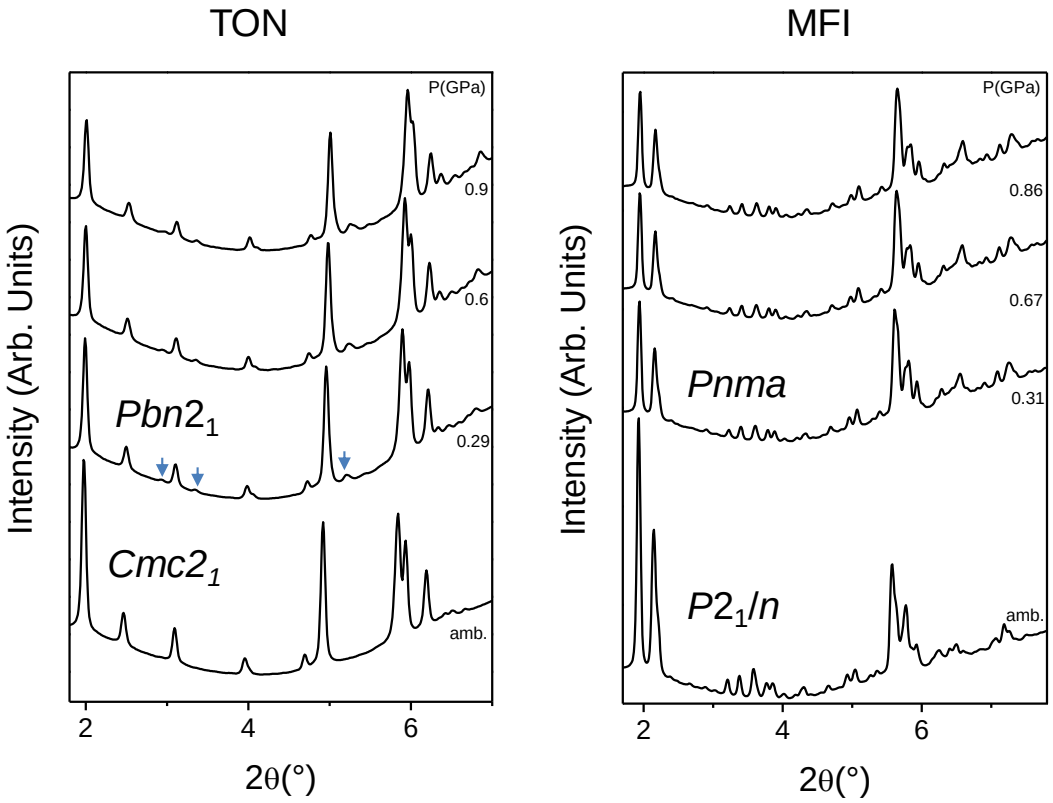

Figure 1. X-ray diffraction patterns of TON and MFI in H_2O on decompression (λ=0.3738 Å). Arrows indicate the principal additional reflections of the *Pbn*2_1 phase.

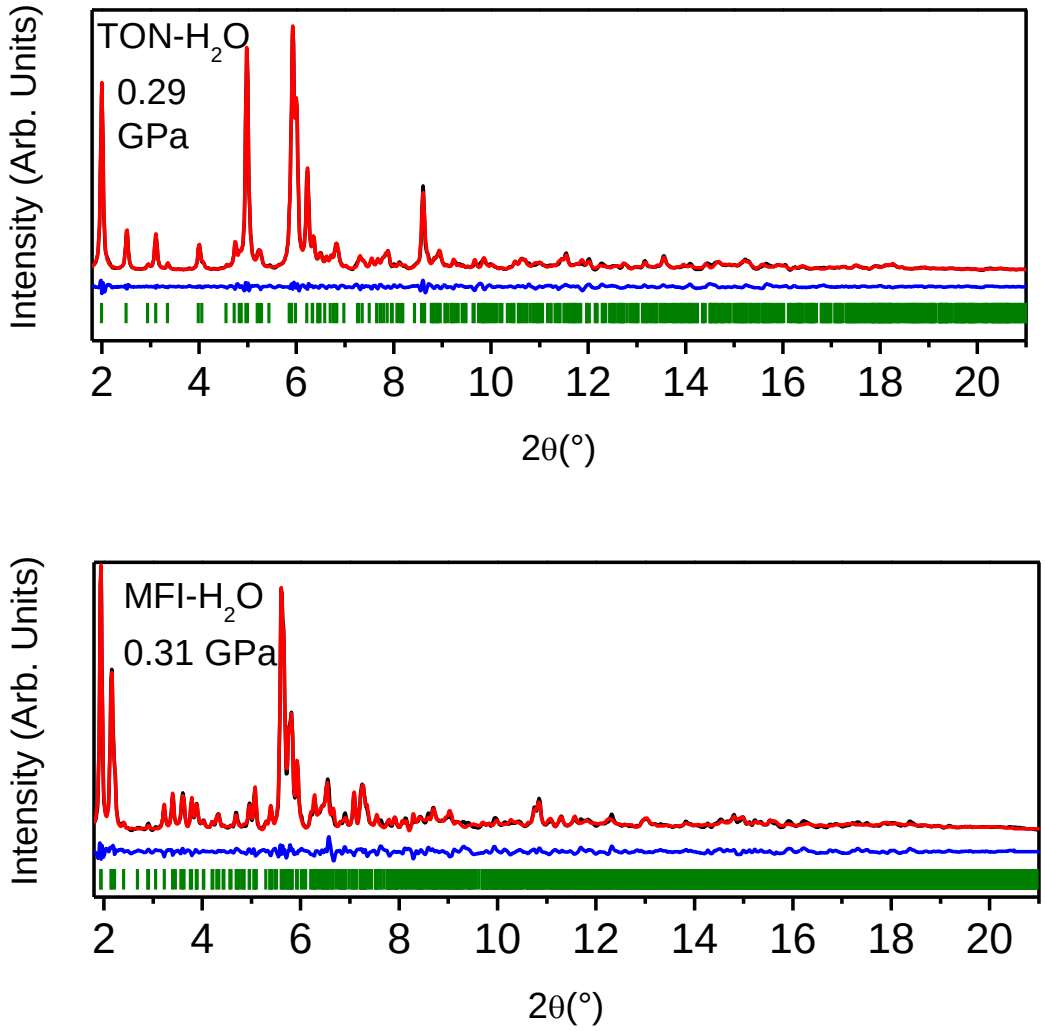

Figure 2. Experimental (black), calculated (red) and difference (blue) profiles (λ=0.3738 Å) for the *Pbn*2_1 structure of TON-H_2O at 0.29 GPa (above) and the *Pnma* structure of MFI-H_2O at 0.31 GPa (below). Vertical bars indicate the calculated positions of the Bragg reflections. The strong background due to Compton scattering from the diamond is subtracted.

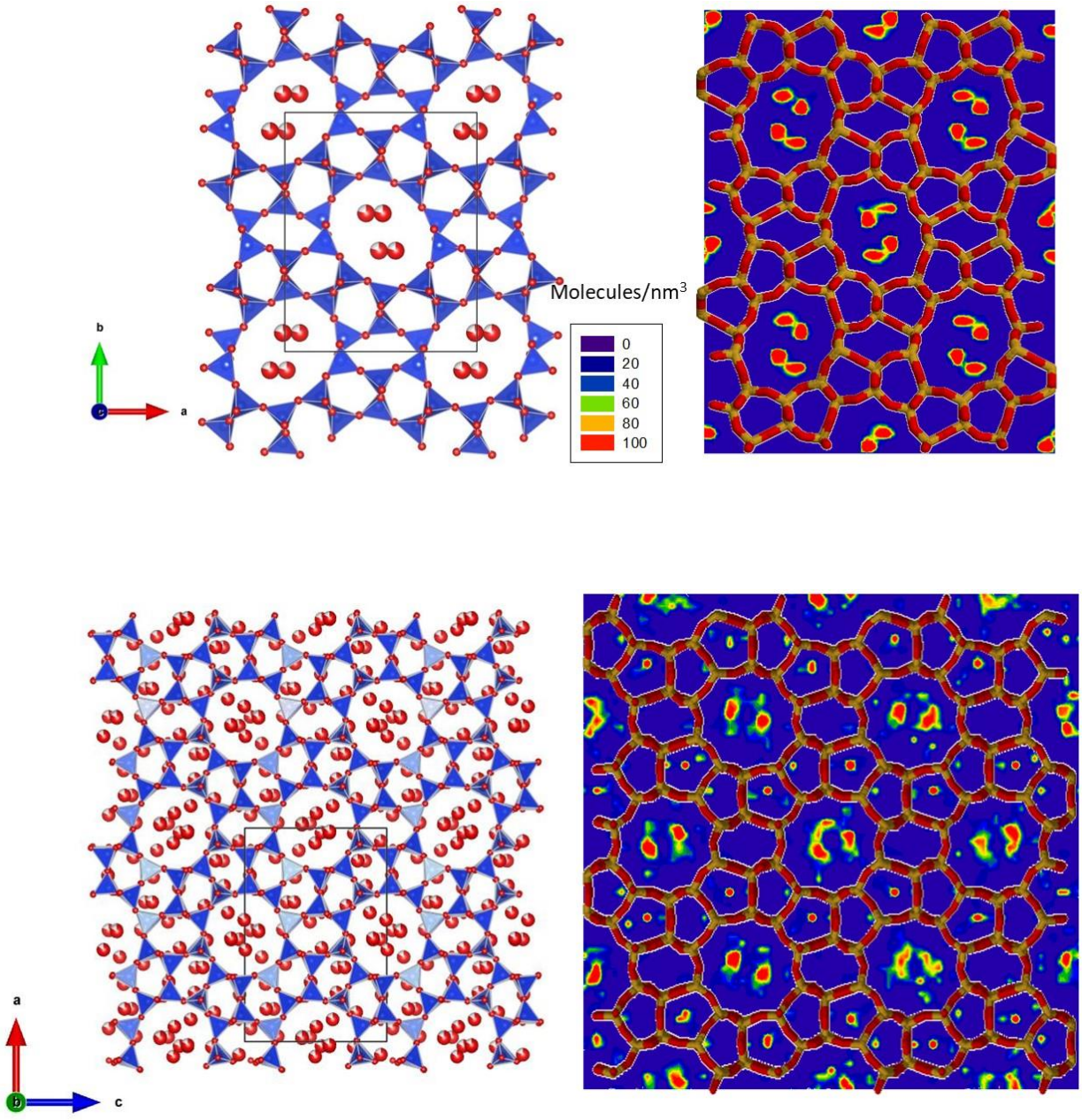

Figure 3. Refined crystal structures (left) and density maps (right) from MC modelling of H_2O-filled TON at 0.29 GPa (*Pbn*2_1) (top) and H_2O-filled MFI at 0.31 GPa (*Pnma*) (bottom). In the crystal structures, the blue and red spheres represent the silicon and oxygen atoms, respectively. In the simulated

data, the color code for the density maps is such that the density increases from purple, blue, green, yellow, orange and red. In the zeolite framework shown for convenience, the orange and red segments indicate chemical bonds that connect the O and Si atoms.

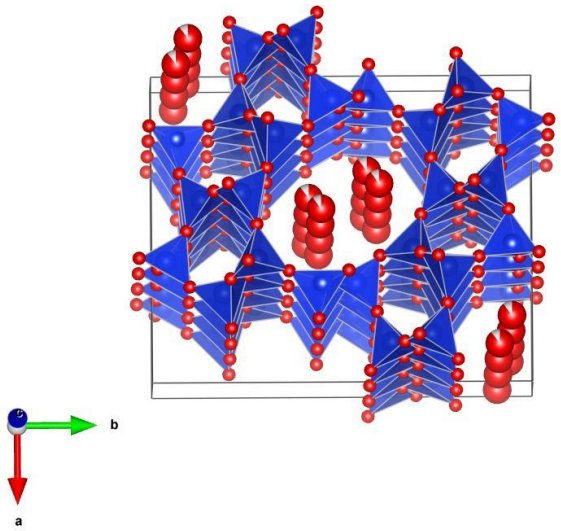

Figure 4. Refined crystal structure of H_2O-filled TON at 0.9 GPa (*Pbn*2_1) showing the chains of H_2O molecules. Blue and red spheres represent the silicon and oxygen atoms, respectively.

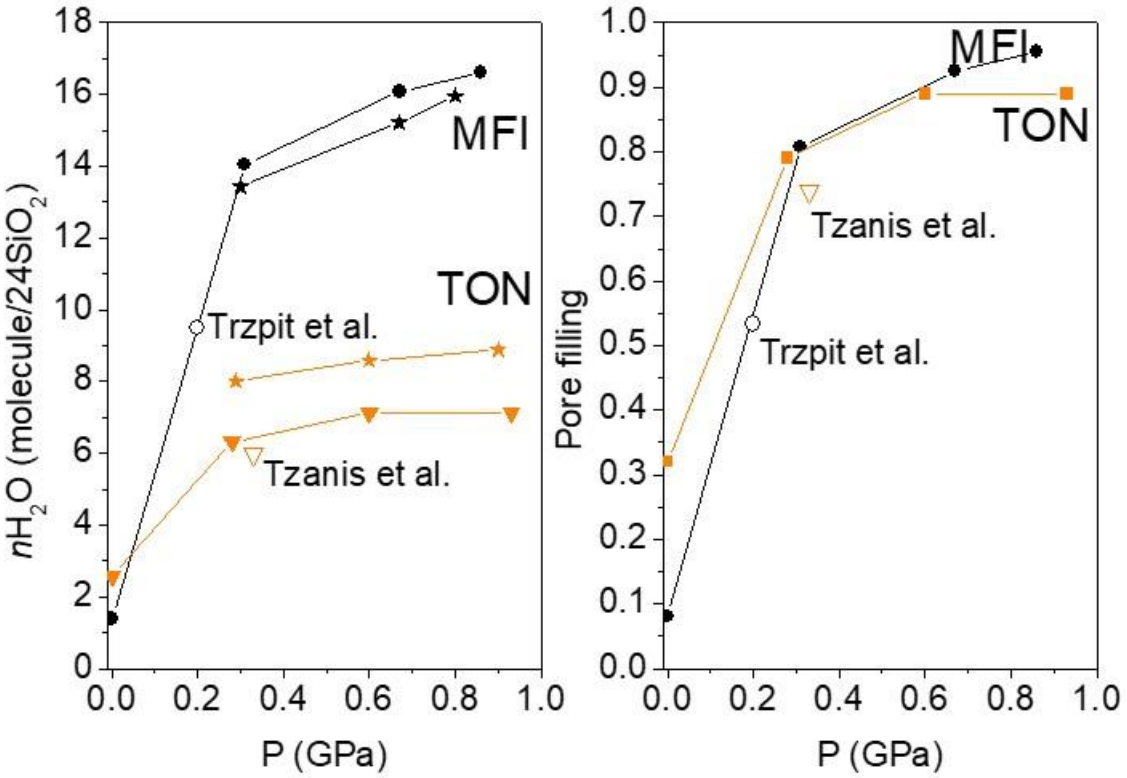

Figure 5. Water content (left) and pore filling (right) of TON (gold symbols) and MFI (black symbols) compressed in water. Experimental (solid symbols) and simulated (stars) data are given in comparison. Empty symbols correspond to bulk H_2O intrusion data from the literature[17, 43].

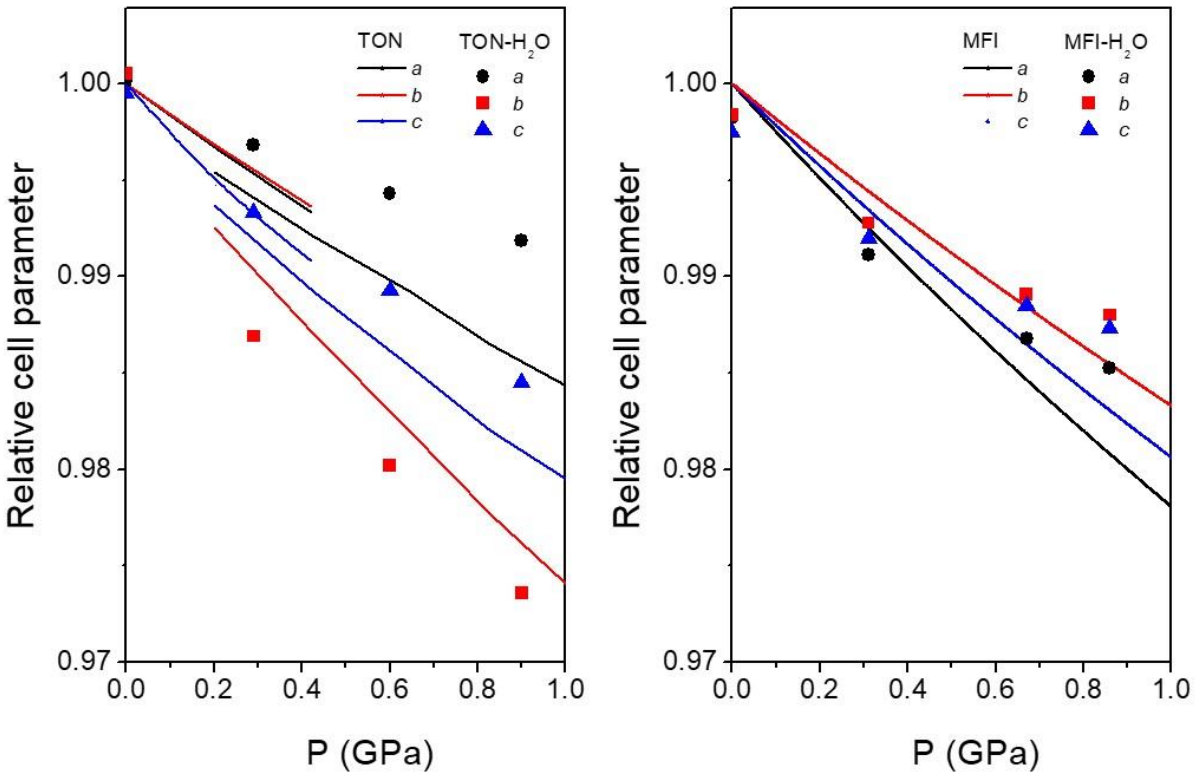

Figure 6. Relative cell parameters of TON and MFI in H_2O as a function of pressure (solid symbols). Continuous lines represent the behavior of TON (orthorhombic phases I and II) and MFI (monoclinic phase) in non-penetrating pressure media[26, 39]. Error bars are smaller than the symbol size.

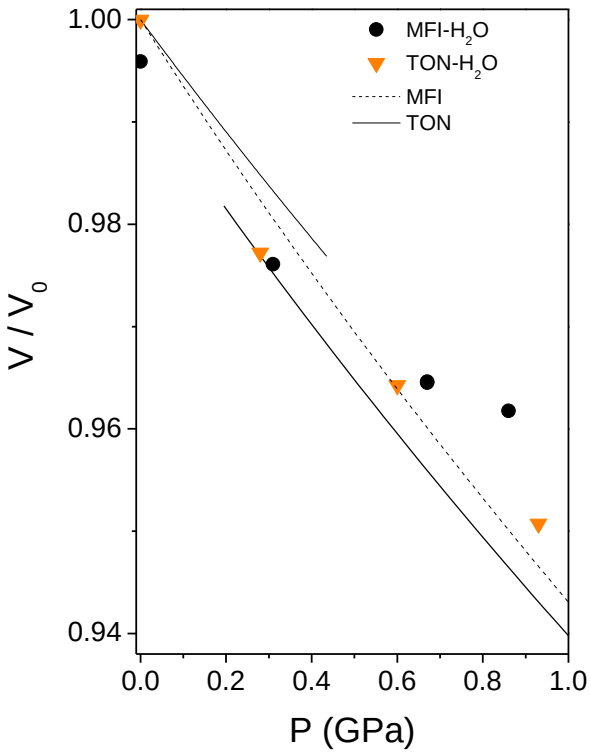

Figure 7. Relative volume (V/V_0) of TON in of TON and MFI in H_2O as a function of pressure (solid symbols). Continuous and dashed lines represents the behavior of TON (orthorhombic phases I and II) and MFI (monoclinic phase) in non-penetrating pressure media[26, 39]. Error bars are smaller than the symbol size.

IR absorption measurements were performed in the H_2O overtone and combination frequency region, since fundamental IR peaks of water were entirely saturated. In Figure 8, we report the IR peaks for the HOH bending + OH stretching (left) and for the double OH stretching (right) vibrational transitions, for pure H_2O, H_2O/TON mixtures and H_2O/MFI mixtures, respectively, at a selected pressure value of 0.8 GPa. In spite of the width of the bands of several hundreds of wavenumbers, which prevents peaks of bulk water and of water confined in the zeolites to be distinguished, it is clear that the peaks corresponding

to overlapping contributions of bulk and confined water are shifted to slightly higher frequencies with respect to those of pure water. In order to provide a quantitative description of microscopic interactions probed by the confined H_2O molecules, we calculated the spectral centroid of the two H_2O IR peaks, that is, the average wavenumber ν_{avg} calculated as $\nu_{avg} = \int \nu A(\nu) d\nu / \int A(\nu) d\nu$, where ν and $A(\nu)$ are the wavenumber and the absorbance, respectively. In Figure 9, we report the pressure shift of the spectral centroid for the two peaks. In all three systems, pure H_2O and the two H_2O/zeolite mixtures, the average frequency linearly decreases upon increasing pressure, which is due to the increasing H-bond at the expense of the covalent O-H bond. More importantly here, the result is that the average frequency for the two H_2O/zeolites is systematically higher than that for pure H_2O, by a few tens of wavenumbers at all pressures. This difference shows that indeed H-bonds in confined water are weaker than in bulk H_2O. This could be due to a longer intermolecular O·····O distance, a O-H·····O angle for the confined molecules differing from 180° and/or disorder in confined water contributing to H-bond weakening by disrupting the ideal tetrahedral arrangement of H-bonds. This disorder of the confined molecules, as a matter of fact, is found to be slightly more pronounced for MFI from MC simulations than for TON. Our MC modelling results give an insight into these different effects.

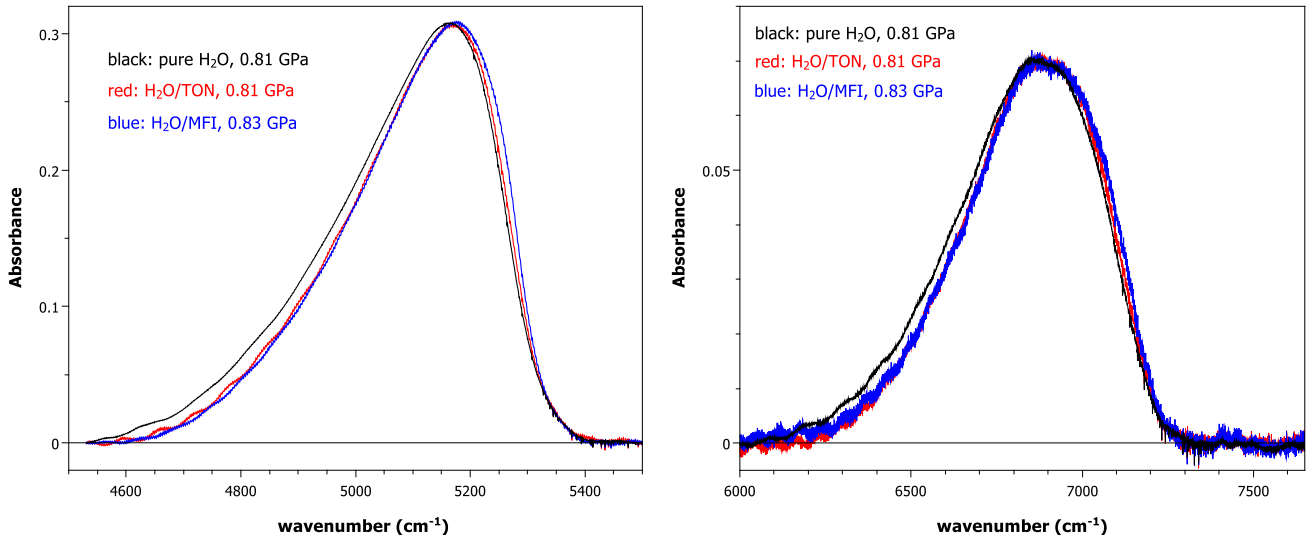

Figure 8. IR absorption spectra in the overtone and combination band spectral regions at a selected pressure, 0.8 GPa, for pure H_2O (black), for a H_2O/TON mixture (red) and for a H_2O/MFI mixture (blue). Left panel: HOH bending + OH stretching peak. Right panel: OH stretching + OH stretching peak. Bands have been normalized to the same peak absorbance.

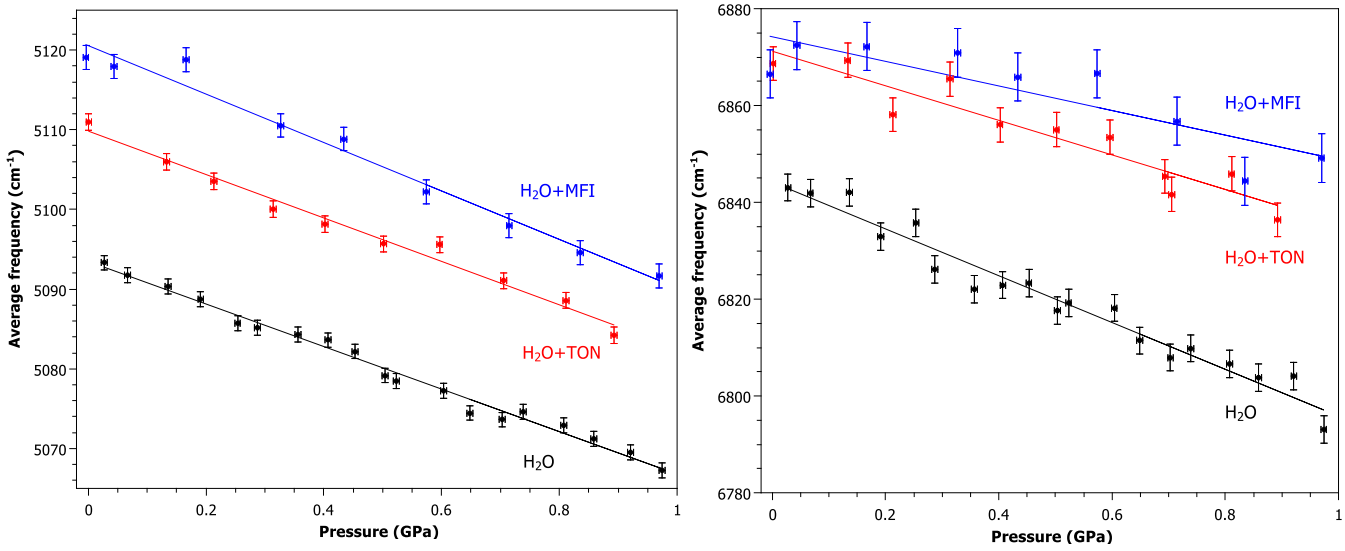

Figure 9. Average frequency, that is the center of mass for the frequencies of the IR overtone and combination peaks (see figure 8) as a function of pressure for: pure H_2O (black), H_2O/TON mixture (red),

and H_2O/MFI (blue). Left panel: HOH bending + OH stretching average frequency. Right panel: OH stretching + OH stretching peak average frequency.

Figure 10 shows the distribution of hydrogen bonding angles < OH-O > and the radial pair distribution function $g(r)$ between O_w atoms in water. These data, which were obtained by means of Grand Canonical Monte Carlo simulations at room temperature and a pressure of 900 MPa, are shown for bulk water and for water confined in MFI and in TON. Both sets of data show that the microscopic structure of confined water differs from bulk water under the same thermodynamic conditions. However, owing to the more severe confinement in its framework, the TON zeolite leads to a more ordered water microscopic structure with more pronounced features/peaks in the angle and radial distributions – compared to the MFI structure. In particular, as shown in Figure 10, while both the orientational (angle distribution) and translational (radial distribution) orderings are affected by nanometric confinement in zeolites, the microscopic structure of water in MFI is less distorted than in TON in the sense that its departs less from that of bulk water under the same thermodynamic conditions (as can be inferred by comparing the amplitude/full width at half maximum for the different systems). These data are consistent with the data by Zhou et al. who showed by means of molecular simulation that, in highly confined environments, even weak water-surface interactions lead to strong perturbations of the intimate water structure[44].

Confined water, which is more ordered in TON, exhibits sharper distributions than in MFI with an average angle closer to 180° corresponding to stronger H-bonds. This is in agreement with the lower IR O-H stretching frequencies for H_2O/TON. An intermediate value for the average angle is obtained for bulk water. The explanation for the stronger H-bond in pure water thus has to be different, and is probably linked to the possibility to have a true tetrahedral environment without the spatial and geometrical constraints of confinement. In all three systems the average O-O distances are very similar indicating that this does not play a major role. This is consistent with the fact that the O-O distance is mostly governed by a

balance between attractive Coulomb/dispersive interactions and short-range steric repulsion, which is only very weakly affected by confinement.

While the simulation data reported in the present paper only focus on thermodynamic/structural aspects, these features are of key importance to account for the rich dynamical/transport properties of water intrusion in hydrophobic media. In particular, the complex structure of water in such ultraconfined environments can be responsible for the mechanisms behaviors observed upon intrusion in all-silica zeolites such as bottleneck effects at the windows of the zeolite structure, broad scattering of residence times, etc.[45]

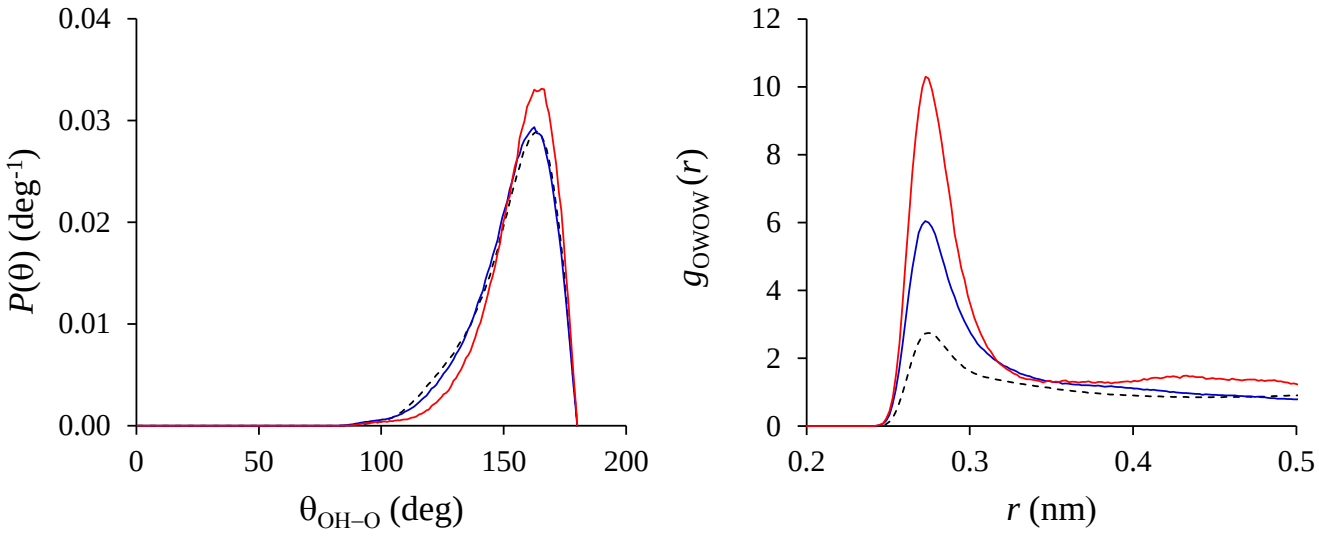

Figure 10. (*left*) Distribution function of hydrogen bonding angles < OH-O > as obtained from Grand Canonical Monte Carlo simulations at room temperature and a pressure of 900 MPa for bulk water (black dashed line) and for water confined in MFI (blue line) and in TON (red line). Pair distribution functions $g(r)$ between O_w atoms as obtained from Grand Canonical Monte Carlo simulations at room temperature and a pressure of 900 MPa for bulk water (black dashed line) and water confined in MFI (blue line) and in TON (red line).

4. Conclusions

The present work indicated that H_2O insertion in TON and MFI zeolites is highly reversible up to 0.9 GPa and that pore filling is essentially complete at this pressure, at which the density of H_2O is essentially identical to liquid water under the same conditions. The structure of inserted H_2O appears more ordered in the 1D pores of TON forming two hydrogen bonded chains, whereas significantly more disorder is observed in the larger pores of the 3D network in MFI. Based on infrared spectroscopy, the hydrogen bonds are weakest in MFI and strongest in liquid water. This can be related to geometric constraints imposed by the pores and disorder, which disrupt the ideal tetrahedral network of H-bonds.

ASSOCIATED CONTENT

Supporting Information. Crystallographic information files (CIF) files containing the structural data for the TON-H_2O system at 0.29, 0.6 and 0.9 GPa and the MFI-H_2O system at 0.31, 0.67 and 0.86 GPa have been supplied as supporting information. This material is available free of charge via the Internet at http://pubs.acs.org..

AUTHOR INFORMATION

Corresponding Author

*Julien Haines

Julien.Haines@umontpellier.fr

Author Contributions

The manuscript was written through contributions of all authors. All authors have given approval to the final version of the manuscript.

Notes

The authors declare no competing financial interests.

ACKNOWLEDGMENT

We acknowledge funding from the Italian Ministry of Education, Universities and Research, MIUR PRIN project ZAPPING, number 2015HK93L7. We also thank the Deep Carbon Observatory (DCO) initiative under the project Physics and Chemistry of Carbon at Extreme Conditions and the Ente Cassa di Risparmio di Firenze under the project Firenze Hydrolab 2.

REFERENCES

1. Hazen, R. M. Zeolite Molecular-Sieve 4A - Anomalous Compressibility and Volume Discontinuities at High-Pressure. *Science* **1983**, *219*, 1065-1067.

2. Lee, Y.; Hriljac, J. A.; Vogt, T.; Parise, J. B.; Artioli, G. First Structural Investigation of a Super-Hydrated Zeolite. *J. Am. Chem. Soc.* **2001**, *123*, 12732-12733.

3. Lee, Y.; Vogt, T.; Hriljac, J. A.; Parise, J. B.; Hanson, J. C.; Kim, S. J. Non-Framework Cation Migration and Irreversible Pressure-Induced Hydration in a Zeolite. *Nature* **2002**, *420*, 485-489.

4. Colligan, M.; Forster, P. M.; Cheetham, A. K.; Lee, Y.; Vogt, T.; Hriljac, J. A. Synchrotron X-Ray Powder Diffraction and Computational Investigation of Purely Siliceous Zeolite Y under Pressure. *J. Am. Chem. Soc.* **2004**, *126*, 12015-12022.

5. Colligan, M.; Lee, Y.; Vogt, T.; Celestian, A. J.; Parise, J. B.; Marshall, W. G.; Hriljac, J. A. High-Pressure Neutron Diffraction Study of Superhydrated Natrolite. *J. Phys. Chem. B* **2005**, *109*, 18223-18225.

6. Seoung, D.; Lee, Y.; Kao, C. C.; Vogt, T.; Lee, Y. Super-Hydrated Zeolites: Pressure-Induced Hydration in Natrolites. *Chem.-Eur. J.* **2013**, *19*, 10876-10883.

7. Arletti, R.; Vezzalini, G.; Morsli, A.; Di Renzo, F.; Dmitriev, V.; Quartieri, S. Elastic Behavior of MFI-Type Zeolites: 1-Compressibility of Na-ZSM-5 in Penetrating and Non-Penetrating Media. *Micropor. Mesopor. Mat.* **2011**, *142*, 696-707.

8. Vezzalini, G.; Arletti, R.; Quartieri, S. High-Pressure-Induced Structural Changes, Amorphization and Molecule Penetration in MFI Microporous Materials: A Review. *Acta Crystallogr. B* **2014**, *70*, 444-451.

9. Arletti, R.; Vezzalini, G.; Quartieri, S.; Di Renzo, F.; Dmitriev, V. Pressure-Induced Water Intrusion in FER-Type Zeolites and the Influence of Extraframework Species on Structural Deformations. *Micropor. Mesopor. Mat.* **2014**, *191*, 27-37.

10. Alabarse, F. G.; Rouquette, J.; Coasne, B.; Haidoux, A.; Paulmann, C.; Cambon, O.; Haines, J. Mechanism of H_2O Insertion and Chemical Bond Formation in $AlPO_4$-54·xH_2O at High Pressure. *J. Am. Chem. Soc.* **2015**, *137*, 584-587.

11. Eroshenko, V.; Regis, R. C.; Soulard, M.; Patarin, J. Energetics: A New Field of Applications for Hydrophobic Zeolites. *J. Am. Chem. Soc.* **2001**, *123*, 8129-8130.

12. Desbiens, N.; Boutin, A.; Demachy, I. Water Condensation in Hydrophobic Silicalite-1 Zeolite: A Molecular Simulation Study. *J. Phys. Chem. B* **2005**, *109*, 24071-24076.

13. Cailliez, F.; Trzpit, M.; Soulard, M.; Demachy, I.; Boutin, A.; Patarin, J.; Fuchs, A. H. Thermodynamics of Water Intrusion in Nanoporous Hydrophobic Solids. *Phys. Chem. Chem. Phys.* **2008**, *10*, 4817-4826.

14. Karbowiak, T.; Paulin, C.; Ballandras, A.; Weber, G.; Bellat, J. P. Thermal Effects of Water Intrusion in Hydrophobic Nanoporous Materials. *J. Am. Chem. Soc.* **2009**, *131*, 9898-9899.

15. Karbowiak, T.; Saada, M. A.; Rigolet, S.; Ballandras, A.; Weber, G.; Bezverkhyy, I.; Soulard, M.; Patarin, J.; Bellat, J. P. New Insights in the Formation of Silanol Defects in Silicalite-1 by Water Intrusion under High Pressure. *Phys. Chem. Chem. Phys.* **2010**, *12*, 11454-11466.

16. Bushuev, Y. G.; Sastre, G. Atomistic Simulation of Water Intrusion-Extrusion in ITQ-4 (IFR) and ZSM-22 (TON): The Role of Silanol Defects. *J. Phys. Chem. C* **2011**, *115*, 21942-21953.

17. Tzanis, L.; Trzpit, M.; Soulard, M.; Patarin, J. High Pressure Water Intrusion Investigation of Pure Silica 1D Channel AFI, MTW and TON-Type Zeolites. *Micropor. Mesopor. Mat.* **2011**, *146*, 119-126.

18. Tzanis, L.; Trzpit, M.; Soulard, M.; Patarin, J. Energetic Performances of Channel and Cage-Type Zeosils. *J. Phys. Chem. C* **2012**, *116*, 20389-20395.

19. Kokotailo, G. T.; Lawton, S. L.; Olson, D. H.; Olson, D. H.; Meier, W. M. Structure of Synthetic Zeolite ZSM-5. *Nature* **1978**, *272*, 437-438.

20. Hay, D. G.; Jaeger, H.; West, G. W. Examination of the Monoclinic Orthorhombic Transition in Silicalite using XRD and Silicon NMR. *J. Phys. Chem.* **1985**, *89*, 1070-1072.

21. Haines, J.; Cambon, O.; Levelut, C.; Santoro, M.; Gorelli, F.; Garbarino, G. Deactivation of Pressure-Induced Amorphization in Silicalite SiO_2 by Insertion of Guest Species. *J. Am. Chem. Soc.* **2010**, *132*, 8860-8861.

22. Ardit, M.; Martucci, A.; Cruciani, G. Monoclinic-Orthorhombic Phase Transition in ZSM-5 Zeolite: Spontaneous Strain Variation and Thermodynamic Properties. *J. Phys. Chem. C* **2015**, *119*, 7351-7359.

23. Barri, S. A. I.; Smith, G. W.; White, D.; Young, D. Structure of Theta-1, the First Unidimensional Medium-Pore High-Silica Zeolite. *Nature* **1984**, *312*, 533-534.

24. Marler, B. Silica-ZSM-22: Synthesis and Single Crystal Structure Refinement. *Zeolites* **1987**, *7*, 393-397.

25. Papiz, M. Z.; Andrews, S. J.; Damas, A. M.; Harding, M. M.; Highcock, R. M. Structure of the Zeolite Theta-1. Redetermination using Single-Crystal Synchrotron-Radiation Data. *Acta Crystallog. C* **1990**, *46*, 172-173.

26. Thibaud, J. M., et al. High-Pressure Phase Transition, Pore Collapse, and Amorphization in the Siliceous 1D Zeolite, TON. *J. Phys. Chem. C* **2017**, *121*, 4283-4292.

27. Thibaud, J. M., et al. Saturation, of the Siliceous Zeolite TON with Neon at High Pressure. *J. Phys. Chem. C* **2018**, *122*, 8455-8460.

28. Di Renzo, F.; Remoue, F.; Massiani, P.; Fajula, F.; Figueras, F. Influence of Diffusional Barriers on the Thermal-Analysis of the Zeolite TON. *Thermochim. Acta* **1988**, *135*, 359-364.

29. Di Renzo, F.; Remoué, F.; Massiani, P.; Fajula, F.; Figueras, F.; Thierry Des, C. Crystallization Kinetics of Zeolite TON. *Zeolites* **1991**, *11*, 539-548.

30. Mao, H. K.; Xu, J.; Bell, P. M. Calibration of the Ruby Pressure Gauge to 800 Kbar under Quasi-Hydrostatic Conditions. *J. Geophys. Res.: Solid Earth* **1986**, *91*, 4673-4676.

31. Prescher, C.; Prakapenka, V. B. Dioptas: A Program for Reduction of Two-Dimensional X-Ray Diffraction Data and Data Exploration. *High Pressure Res.* **2015**, *35*, 223-230.

32. Rodriguez-Carvajal, J. Magnetic Structure Determination from Powder Diffraction Using the Program Fullprof. *Applied Crystallogr.* **2001**, 30-36.

33. Momma, K.; Izumi, F. Vesta 3 for Three-Dimensional Visualization of Crystal, Volumetric and Morphology Data. *J. Appl. Crystallogr.* **2011**, *44*, 1272-1276.

34. Gorelli, F. A.; Ulivi, L.; Santoro, M.; Bini, R. The Epsilon Phase of Solid Oxygen: Evidence of an O_4 Molecule Lattice. *Phys. Rev. Lett.* **1999**, *83*, 4093-4096.

35. Coasne, B.; Ugliengo, P. Atomistic Model of Micelle-Templated Mesoporous Silicas: Structural, Morphological, and Adsorption Properties. *Langmuir* **2012**, *28*, 11131-11141.

36. Mishima, O.; Endo, S. Phase-Relations of Ice under Pressure. *J. Chem. Phys.* **1980**, *73*, 2454-2456.

37. Zhang, K.; Lively, R. P.; Noel, J. D.; Dose, M. E.; McCool, B. A.; Chance, R. R.; Koros, W. J. Adsorption of Water and Ethanol in MFI-Type Zeolites. *Langmuir* **2012**, *28*, 8664-8673.

38. Koster, H.; Franck, E. U. Das Spezifische Volumen Des Wassers Bei Hohen Drucken Bis 600°C Und 10 Kbar*) *Ber. Bunsen. Phys. Chem.* **1969**, *73*, 716-722.

39. Haines, J.; Levelut, C.; Isambert, A.; Hébert, P.; Kohara, S.; Keen, D. A.; Hammouda, T.; Andrault, D. Topologically Ordered Amorphous Silica Obtained from the Collapsed Siliceous Zeolite, Silicalite-1-F: A Step toward "Perfect" Glasses. *J. Am. Chem. Soc.* **2009**, *131*, 12333-12338.

40. Coasne, B.; Haines, J.; Levelut, C.; Cambon, O.; Santoro, M.; Gorelli, F.; Garbarino, G. Enhanced Mechanical Strength of Zeolites by Adsorption of Guest Molecules. *Phys. Chem. Chem. Phys.* **2011**, *13*, 20096-20099.

41. Krishna, R.; van Baten, J. M. In Silico Screening of Zeolite Membranes for CO_2 Capture. ***J. Membrane Sci.*** **2010**, *360*, 323-333.

42. Flanigen, E. M.; Bennett, J. M.; Grose, R. W.; Cohen, J. P.; Patton, R. L.; Kirchner, R. M.; Smith, J. V. Silicalite, a New Hydrophobic Crystalline Silica Molecular-Sieve. *Nature* **1978**, *271*, 512-516.

43. Trzpit, M.; Soulard, M.; Patarin, J.; Desbiens, N.; Cailliez, F.; Boutin, A.; Demachy, I.; Fuchs, A. H. Influence of Defects on the Water Intrusion in Silicalite-1 Zeolite: Confrontation of Experimental and Molecular Simulation Results. *Zeolites and Related Materials: Trends, Targets and Challenges, Proceedings of the 4th International Feza Conference* **2008**, *174*, 561-564.

44. Zhou, T. C.; Bai, P.; Siepmann, J. I.; Clark, A. E. Deconstructing the Confinement Effect Upon the Organization and Dynamics of Water in Hydrophobic Nanoporous Materials: Lessons Learned from Zeolites. *J. Phys. Chem. C* **2017**, *121*, 22015-22024.

45. Turgman-Cohen, S.; Araque, J. C.; Hoek, E. M. V.; Escobedo, F. A. Molecular Dynamics of Equilibrium and Pressure-Driven Transport Properties of Water through LTA-Type Zeolites. *Langmuir* **2013**, *29*, 12389-12399.

TOC Graphic